Sulfonated MCM-41 as potential catalyst to obtain biolubricants from vegetable oil

Aurélia R. O. Ferreira[a], Joaquín Silvestre-Albero[b], Martin E. Maier[c], Nágila M. P. S. Ricardo[d], Célio L. Cavalcante Jr[a] and F. Murilo T. Luna[a†]

[a]Núcleo de Pesquisas em Lubrificantes, Grupo de Pesquisa em Separações por Adsorção, Depto. de Engenharia Química, Universidade Federal do Ceará, Campus do Pici, Bl. 709, Fortaleza, CE, 60440-900, Brazil.

[b]Laboratorio de Materiales Avanzados, Depto. de Química Inorgánica, Universidad de Alicante, E-03690 San Vicente del Raspeig, Spain.

[c]Fachbereich Chemie, Institut für Organische Chemie, Auf der Morgenstelle 18,Tübingen, 72076, Germany.

[d]Laboratório de Polímeros e Inovação de Materiais, Depto.de Química Orgânica e Inorgânica, Universidade Federal do Ceará, Campus do Pici, Bl. 940, Fortaleza, CE, CEP 60440-900, Brazil.

[†] Corresponding author (Phone: +55-85-3366-9611, Fax: +55-85-3366-9601, e-mail: murilo@gpsa.ufc.br)

ABSTRACT

Biolubricants may be obtained from vegetable oils using appropriate chemical modifications, to improve their physicochemical properties for lubrication applications. In this study, the esterification of a free fatty acid (FFA) with long chain alcohols was performed using sulfonated mesoporous silica as catalyst. Fresh and functionalized MCM-41 samples were prepared to evaluate the effect of the sulfonic surface group on the esterification reaction. MCM-41 was functionalized via post-synthesis modification using 3-mercaptopropyltrimethoxysilane (MPTS) as silylating agent. The synthesized catalysts were characterized using several techniques. After the functionalization, a decrease in the apparent surface area and pore diameter were observed. The MCM-41/SO_3H sample was applied in the esterification reaction of oleic acid (as a FFA model) using two different long-chain alcohols (octanol and 2-ethylhexanol). The catalytic results reveal that sulfonated catalyst showed excellent conversions (~100% mol when using octanol and >93% mol using 2-ethylhexanol) and selectivities to esters (*ca.* 90%).

Keywords: mesoporous materials; MCM-41; heterogeneous catalysis; esterification; fatty acids.

1. INTRODUCTION

Alternative routes to obtain lubricants using renewable sources have been attracting intense research studies lately. Besides the environmental benefit, bio-based lubricants obtained from vegetable oil may present very good lubricity characteristics and other physicochemical properties (Owuna et al. 2020). Vegetable oils present some advantages over mineral oil, such as better lubricating effects, biodegradable nature, high viscosity index and low volatility. However, they present very low chemical stability and thus must undergo chemical modifications to be used as biolubricants (Owuna et al. 2020; Madankar, Dalai and Naik 2013). These modifications may be carried out by esterification of free fatty acids (FFA) obtained from a vegetable oil using a long-chain alcohol to allow appropriate properties for eventual lubricant applications (Saboya et al. 2017).

Several studies have been reported using esterification reactions between FFA and long-chain alcohols, such as 2-ethylhexanol (Ferreira et al. 2020; Oliveira et al. 2020; Saboya et al. 2017; Russo et al. 2021; Pindit et al. 2021; Salimon, Salih and Yousif 2012). As well known, using heterogeneous instead of homogeneous catalysts convey several advantages, such as reduction in waste water, catalyst recovery and mitigation of potential corrosion problems in plant equipment (Radhakrishnan et al. 2011).

MCM-41 material belongs to a family of silicas called M41S that were discovered in the 90s by researchers at Mobil R&D Corp. These were the first materials containing ordered and uniform mesoporous structures, with a narrow pore size distribution (Blin and Su 2002; Vartuli et al. 1994; Wang et al. 2013; Ciriminna et al. 2014; Al-Hazmi and Apblett 2011). These materials emerged from the need to process bulky molecules, a problem that microporous molecular sieves were not able to address due to their small pore diameter. Thereby, these materials have attracted attention of researchers over the world due their

excellent properties, such as high surface area, regular pore shape, large pore volume, narrow pore size distribution, tunable pore size (Chermahini et al. 2015).

For catalytic applications, modification of the surface chemistry in MCM-41 is mandatory due to the low acidity of the silanol (Si-OH) groups. To this end, the silanol groups play a major role since these will be used as anchoring sites for the desired functionality. Based on this concept, many researchers have been studying the incorporation of functional groups, thus generating Brønsted and/or Lewis acid sites upon request (Kister et al. 2012; Ding et al. 2018; Wagh et al. 2018; Tayade et al. 2015; Piscopo et al. 2012).

MCM-41 functionalization may be carried out through a direct synthesis route, which involves a one-step strategy based on co-condensation from two sources of silicas, or via post-synthesis modification. The latter approach involves the surface modification by grafting or coating (Liu et al. 2009; Huang et al. 2016; Wang et al. 2019; Krishna et al. 2018; Noda et al. 2016). Several studies have described the efficiency in the insertion of acidic groups on the surface of MCM-41 for application in catalysis (Chermahini et al. 2015; Díaz et al. 2005; Wang et al. 2017; Rossetto et al. 2018; Mohino et al. 2002; Debasish, Jyh-Fu Lee and Cheng 2001). Some studies described that this material has an efficient catalytic performance when applied in esterification reactions, due to the combination of high acidity and proper porous structure (Díaz et al. 2005; Díaz et al. 2001; Díaz et al. 2001). However, to our knowledge, the activity of sulfonated MCM-41 as a potential catalyst for the esterification of FFA, using long-chain alcohols for biolubricants synthesis, has not been reported in the open literature.

In this study, a fresh MCM-41 sample was synthesized using a standard reported method. That sample was then functionalized with sulfonic groups, via post-synthesis modification using 3-mercaptopropyltrimethoxysilane (MPTS) as silylating agent, followed by oxidation with H_2O_2. The MCM-41 samples (non-functionalized and functionalized) were characterized using several techniques. Then the catalysts were evaluated in the esterification

of oleic acid using two different long-chain alcohols (octanol and 2-ethylhexanol). The reaction conversions and selectivities were monitored using Nuclear Magnetic Resonance (H^1 NMR).

2. EXPERIMENTAL SECTION

2.1. Materials

Tetraethyl orthosilicate (TEOS, 98% wt.), 3-mercaptopropyltrimethoxy-silane (MPTS), chloroform-d (CDCl3, 99.8%) and trimethylolpropane (>98% wt.) were purchased from Sigma-Aldrich (USA). The oleic acid (90% wt., Sigma-Aldrich/USA) was used as free fatty acid model for the esterification reactions. Cetyltrimethylammonium bromide (99% wt.) was provided by Vetec (Brazil). Octanol (>99% wt.) and 2-ethylhexanol (≥ 99% wt.) were purchased from Merck (Germany). The hydrogen peroxide (35% wt.) was provided by Dinâmica (Brazil) and the ethyl acetate (≥ 99% wt.) was purchased from Fluka (Germany).

2.2. Preparation and functionalization of mesoporous silica

The procedure to obtain the MCM-41-type mesoporous silica was modified from Araújo et al. (2013), with a reaction mixture composition as shown in Eq. 1. The moles of ethanol in the composition refer to the hydrolysis of the silica source (TEOS). The obtained silica material was then calcined in three steps: first, at 150 °C with a heating rate of 5 °C/min for 2 h; second, at 300 °C, 10 °C/min for 2 h; and third at 550 °C in heating rate 10 °C/min for 5 h, as previously reported by Campos et al. (2020).

$$1\ SiO_2{:}0.3\ CTABr{:}0.5\ NaOH{:}144\ H_2O{:}4\ EtOH \qquad \text{(Eq. 1)}$$

MPTS was used as organosilane in the silylation reaction and the procedure was adapted from Borrego et al. (2010). The silylation was carried out in N_2 atmosphere under reflux. Approximately 0.8 g of MCM-41 was added into 19.6 mL of a solution of the dry toluene and MPTS (10% wt.), the

105 reaction medium was stirred for 24 h at 85 °C. After that, the material was washed with acetone and
106 toluene, and then it was dried for 12 h at 100 °C.

107 The oxidation of the –SH group (Scheme 1) was carried out with H_2O_2. Briefly, 0.78 g of
108 material was added into approximately 15 mL of H_2O_2 (ratio solid:liquid of 1:20 g/ml) and the mixture
109 was stirred at 60 °C for 24 h. The catalyst sample was separated by filtration, washed with distilled
110 water and then the material was acidified with 0.1 M H_2SO_4. This treatment aims to assure total
111 oxidation of the thiol groups (-SH) that might not have been completely oxidized in the previous step
112 with H_2O_2. Finally, the sample was washed with distilled water to remove all traces of liquid acid.
113 Then, the catalyst was dried for 12 h at 60 °C (Debasish, Jyh-Fu Lee and Cheng 2001).

114

115 **<Scheme 1>**

116

117 *2.3. Characterization of catalyst samples*

118 The textural properties of the prepared catalyst samples were characterized using nitrogen
119 adsorption/desorption at –196 °C in an Autosorb IQ3 equipment from Quantachrome Instruments
120 (USA). Approximately 40 mg of sample is degassed under vacuum using a turbo-molecular pump,
121 heated from room temperature to 150 °C for 6 hours under heating rate of 1 °C/min. The specific
122 surface area (S_{BET}) was calculated using the BET method (relative pressures between 0.1 and 0.3) and
123 the total pore volume was obtained from the N_2 volume adsorbed at a relative pressure of 0.95. The
124 pore size distributions were calculated using the density functional theory method (DFT), following
125 the approach reported by Jagiello and Thommes (2004).

126 The X-Ray Diffraction was carried out in the Bruker D8-Advance with Göebel mirror (non-
127 flat samples) with high temperature chamber (up to 900 °C), with an X-ray generator
128 KRISTALLOFLEX K 760-80 F (Power: 3000 W, Voltage: 20-60 KV and Current: 5-80 mA) equipped
129 with an RX tube with copper anode. The distance between the planes of the synthesized material was

estimated from Equation 2, where the Bragg angle (θ) is given by the diffractogram and the lattice parameter (a_0), calculated using the Equation 3 (Campos et al. 2020).

$$d=(n.\lambda)/(2.\sin\theta) \quad \text{(Eq. 2)}$$

$$a_{100}= (2.d_{100})/\sqrt{3} \quad \text{(Eq. 3)}$$

A transmission electron microscope (TEM) model JEOL JEM-1400 Plus (Japan), that works at 120 keV and is equipped with an Orius camera (Gatan), was used for image acquisition. The resolution achieved is 0.38 nm between points and 0.2 nm between lines. It has four grid holders, which saves time when changing samples. A scanning electron microscope (Hitachi S3000N, Japan) equipped with an X-ray detector Bruker XFlash 3001 for microanalysis (EDS) was used to characterize the catalysts. The scanning microscope is able to work in variable pressure mode for observation of nonconductive specimens without coating of samples.

A spectrometer K-ALPHA of Thermo Scientific (USA) was used to measure the X-ray photoelectron spectra of the catalysts. All spectra were collected using Al-Kα radiation (1486.6 eV), monochromatized by a twin crystal monochromator, yielding a focused X-ray spot (elliptical in shape with a major axis length of 400 μm) at 3 mA × 12 kV. The alpha hemispherical analyzer was operated at 200 eV and 50 eV to measure the whole energy band and to measure the particular elements. The C 1s core level was used as reference binding energy, and it is located at 284.6 eV. The samples were pressed and mounted on the sample holder and placed in the vacuum chamber. Before recording the spectrum, the samples were maintained in the analysis chamber until a residual pressure of *ca.* 5×10^{-7} N/m^2 was reached. The quantitative analysis was estimated by calculating the integral of each peak, after subtracting the S-shaped background, and by fitting the experimental curve to a combination of Lorentzian (30%) and Gaussian (70%) lines.

The infrared spectra were recorded on an ABB Bomem FTLA 2000-102 FTIR instrument (USA). The spectra were acquired by accumulating 100 scans at 4 cm^{-1} resolutions in the range of 400-4000 cm^{-1} using samples (2 wt.%) with KBr.

Thermal stability of catalysts was measured by thermal gravimetric analysis (TGA-QMS customized, model STA 409 CD/403/5/G SKIMMER – Netzsch, Germany) with a heating ramp of 10 °C/min, from 30 °C to 800 °C.

2.4. Catalytic activity

The catalytic activity of the synthesized samples was evaluated in the esterification of oleic acid (OA) using different long-chain alcohols: octanol and 2-ethylhexanol (see Scheme 2). The reaction was carried out under inert atmosphere at 90 °C in a three-neck round bottom reactor, using a mass ratio of 4:100 (catalyst to oleic acid), as previously reported by Ferreira et al. (2020). This was performed for 6 h under agitation of 500 rpm, which should eliminate any external mass transfer constraints (Russo et al. 2021).

<Scheme 2>

First, the oleic acid (3.0 g, for molar ratio 1:4 OA:alcohol) was heated to 90 °C and then the long-chain alcohol was added in the appropriate molar ratios. After that, the catalyst sample (MCM-41 or MCM 41/SO_3H) was added to the reaction medium and samples were then collected at given time intervals.

The evaluation of the reaction products was carried out by Nuclear Magnetic Resonance of Hydrogen (^{1}H NMR) using a Bruker spectrometer (AVANCE model) operating at a frequency of 400 MHz. The solvent used for these analyses was deuterated chloroform at a temperature of 25 °C. The peak of the -CH_2- bond, at 2.25-2.5 ppm, was taken as reference for monitoring the conversion of oleic acid and the peak for the -HC=CH- bond was used for calculation the selectivity in oleate by the Equations 4-6:

$$CO=(a_1/2).100\% \quad \text{(Eq. 4)}$$

$$DC = ((2-a_2)/2).100\% \quad \text{(Eq. 5)}$$

$$S = CO/(CO+DC).100\% \quad \text{(Eq. 6)}$$

where: a_1 is the area of the new binding peak, concerning $–CH_2–$ bond, approximately 4.0 ppm; a_2 is the peak area of double bond, approx. 5.5 ppm; CO is the conversion (% mol) to oleate; DC is the double bond conversion (% mol) and S is the selectivity for oleic ester (Ferreira et al. 2020).

3. RESULTS AND DISCUSSION

3.1. Characterization of catalysts

The nitrogen adsorption and desorption isotherms at –196 °C of the catalysts are shown in Figure 1a (data included in Table 1). The catalysts exhibited a type IV isotherm, according to the IUPAC classification (González et al. 2012), with narrow H4 type hysteresis. As shown in Table 1, the specific surface area (S_{BET}) decreases from 855 m^2/g, in the original MCM-41 sample, to 600 m^2/g, after the anchoring of the sulfonic groups. The total pore volume also decreased significantly (from 0.71 to 0.39) after the funcionalization. Furthermore, changes in the porous structure are also evident from the pore size distributions (PSD) shown in Figure 1b. The PSD curve of the fresh material indicates pore sizes predominantly in the range between 2 and 4 nm, whereas the functionalized sample presented a shift of those pore sizes to a lower range (between 1.5 and 3.3 nm). Debasish et al. (2001) reported the reduction in the pore diameter of MCM-41 after functionalization, this observation being a clear proof of the successful anchoring of the sulfonic groups within the mesoporous tubes, with no deterioration of the mesoporous network.

<Figure 1>

<Table 1>

Although MCM-41 silicas are amorphous solids (long-range) and do not exhibit a well-defined XRD pattern, as compared to zeolites (Figure 2a,b and Figure 3), they present a short-range order due to the hexagonal arrangement of the mesopores, thus explaining the XRD peaks observed at low 2 θ values. As seen in Figures 2c-f, the modification with the organosilane apparently has not affected the morphology of the catalyst. Nevertheless, the XRD's presented in Figure 3 display peaks at low angle in both curves showing greater intensity in the sample without modification (black line). The MCM-41/SO_3H silica showed a lower intensity at the same peak (around 3 θ) which indicates that the functionalization was indeed carried out. However, there was no displacement of the peak which means that the values of the interplanar distance and the hexagonal arrangement parameter (d_{100} and a_0, respectively) are essentially the same as in the fresh MCM-41 sample (see Table 1).

<Figure 2>

<Figure 3>

The sample which was oxidized to obtain the –SO_3H groups was assessed by high-resolution X-ray photoelectron spectroscopy to assess the presence the sulfonic groups. In Figure 4 it may be seen that the XPS spectrum contains peaks between 168–172 eV, which correspond to oxidized sulfur in an anchored –SO_3H species (González et al. 2012; Valle-Vigón, Sevilla and Fuertes 2012).

<Figure 4>

The FTIR spectroscopy (Figure 5) was carried out as additional analysis to the XPS to confirm the anchoring of the sulfonic groups. The spectrum shows a broad band at 1080 cm^{-1}

that represents the antisymmetric vibration of the Si-O bond, in that same region one would also expect sulfonic acid bonds, which would be attributed to the O=S=O and S=O, asymmetric and symmetric stretching, respectively (Chermahini et al. 2015). Approximately at 970 cm^{-1} the vibrational band can be assigned to Si-O-Si, the broad band between 3100 and 3700 cm^{-1} is assigned to hydroxyl groups both in silanols and water (Kister and Roessner 2012). The MCM-41 sample (Figure 5, black line) used in this analysis has organic material inside of pores (CTA^+, surfactant CTABr without the bromide ion). Then the vibration bands at 2900 and 1470 cm^{-1} are related to bond C–H stretches that come from the surfactant used to synthesize the material (Reyes et al. 2015).

<Figure 5>

The thermal stability of the catalyst samples was measured by TG (see Figure 6). A weight loss up to 100 °C may be identified for both samples, attributed to the loss of adsorbed water. In Figure 6a, it may be observed a more level of loss weight, where up to 350 °C is attributed to the elimination of organic material from CTA^+ (surfactant) (Díaz et al. 2001). Above this temperature, the weight loss may be attributed to condensation of the silanol groups thus releasing H_2O. For the sulfonated sample (Figure 6b), only two levels of weight loss were detected, one for water at 100 °C (as already mentioned) and other between 200 °C and 500 °C, due to the decomposition of sulfonic groups which occurs up to approximately 350 °C (Debasish, Jyh-Fu Lee and Cheng 2001).

<Figure 6>

3.2. Catalytic experiments

The conversions and selectivities were monitored using Nuclear Magnetic Resonance of Hydrogen (^{1}H NMR). The spectra of samples obtained from the esterification reaction of oleic acid with octanol and 2-ethylhexanol are shown in Figure 7. The oleic acid molecule has in its chemical structure two highly reactive functional groups: terminal carboxyl group (2.25-2.5 ppm) and unsaturation at ninth carbon (~5.5 ppm). The esterification reaction is confirmed in Figure 7 with the appearance of ester peak at ~4.0 ppm, corresponding to hydrogen of the CH_2 group attached to the oxygen of the ester. The conversion values were calculated using the area of the acid function peak as reference (equals to 2.00 ppm).

<Figure 7>

Oleic acid conversions versus reaction time (up to six hours) for all samples are shown in Figure 8. For all experiments, the non-functionalized MCM-41 sample exhibits a low catalytic activity in the oleic acid esterification, with maximum conversion values around 20 % mol. On the contrary, the conversion of oleic acid using the MCM-41/SO_3H sample was above 90 % mol after 3 h for both alcohols. The functionalized MCM-41 sample presents excellent conversion values (*ca.* 100% when using octanol and above 93 % when using 2-ethylhexanol) after 6 h of reaction.

<Figure 8>

It may be observed that, when using the MCM-41/SO_3H sample, there is a decreasing trend in conversion with increasing branching level of the alcohols. This is related to the higher steric hindrance in the molecules of 2-ethylhexanol that causes a reduction in the interaction between the FFA and alcohol in the active sites of catalysts. High ester selectivities were

obtained (ca. 90%) for both alcohols in the MCM-41/SO3H sample, as shown in Table 2, much higher than the values obtained for the non-functionalized samples.

<Table 2>

However, for the MCM-41/SO_3H sample, the ester selectivity, using 2-ethylhexanol, was slightly higher than that observed for octanol. A reported mechanism for the esterification of FFA using heterogeneous acid catalysts (Fraile et al., 2015) consists of three steps: initial protonation of the FFA, followed by an attack of the alcohol on the carbocation, leading to a tetrahedral intermediate, and, finally, water elimination, resulting in the catalyst regeneration. The slightly higher selectivity of 2-ethylhexanol when compared to n-octanol for the MCM-41/SO_3H sample may be related to a likely lower packing of the branched alcohol molecules (compared to linear molecules), which makes the attack of the FFA carbocation slightly more favorable, thus improving the ester selectivity.

For non-functionalized sample, the values of selectivities to esters showed decreasing trend with increasing branching level of alcohols. The sulfonated MCM-41 showed better performances than fresh sample for both alcohols. Thus, the selectivity to esters increased with the presence of the sulfonated catalyst, in all cases in such a way that the modified catalyst exhibited a selectivity trend (2-ethylhexyl oleate > octyl oleate) after 6 h of reaction.

4. CONCLUSIONS

MCM-41 mesoporous silica was synthesized and then modified by post synthesis using MPTS as silylating agent to obtain MCM-41/SO_3H. The results of N_2 physisorption and XRD showed that the modification on the MCM-41 effectively took place. Furthermore, SEM/TEM and XRD results indicated that the mesoporous arrangement did not change with the presence

of the sulfonic group. The -SO_3H on the surface of the mesoporous silica was confirmed by XPS through the peak around 170 eV which is the binding energy of sulfonic groups.

The catalyst samples were applied in the esterification reaction of oleic acid with two different alcohols and the MCM-41/SO_3H sample exhibited promising results in the catalytic activity. In contrast, the original MCM-41 sample had much lower catalytic activity when compared to the sulfonated sample. The conversion values for MCM-41/SO_3H reached ~100% mol when using octanol and >93% mol when using 2-ethylhexanol. The selectivity to obtain esters was improved when sulfonated MCM-41 was used. Despite the branching of 2-ethylhexanol, the MCM-41/SO_3H was more selective in the esterification reaction reaching *ca.* 90 % for 2-ethylhexyl oleate.

DECLARATION OF INTERESTS

The authors declare that they have no known competing financial interests or personal relationships that could have appeared to influence the work reported in this paper.

ACKNOWLEDGMENT

The authors wish to acknowledge the financial support provided by FUNCAP (*Fundação Cearense de Apoio ao Desenvolvimento Científico e Tecnológico*) and CNPq (*Conselho Nacional de Desenvolvimento Científico e Tecnológico*). This study was financed in part by the CAPES (*Coordenação de Aperfeiçoamento de Pessoal de Nível Superior*) – Brazil, Finance Code 001. Also, financial support from GV (PROMETEOII/2014/004), MINECO (MAT2016-80285-p) and H2020 (MSCA-RISE-2016/NanoMed Project) is gratefully acknowledged.

REFERENCES

Al-Hazmi MH, Apblett AW (2011) Benzylation of benzene over sulfated zirconia supported in MCM-41 using a single source precursor, Catal. Sci. Technol. https://doi.org/10.1039/C1CY00004G

Araújo JA, Cruz FT, Cruz IH, Cardoso D (2013) Encapsulation of polymers in CTA-MCM-41 via microemulsion, Micropor. Mesopor. Mat. https://doi.org/10.1016/j.micromeso.2013.05.010

Blin JL, Su BL (2002) Tailoring Pore Size of Ordered Mesoporous Silicas Using One or Two Organic Auxiliaries as Expanders, Langmuir. https://doi.org/10.1021/la020042w

Borrego T, Andrade M, Pinto ML, Silva AR, Carvalho AP, Rocha J, Freire C, Pires J (2010) Physicochemical characterization of silylated functionalized materials, J. Colloid Interf. Sci. https://doi.org/10.1016/j.jcis.2010.01.026

Campos AFP, Ferreira ARO, Silva LL, Neto PPM, Cardoso D (2020) Synthesis and properties of hybrid silicas containing alkylammonium surfactants, Catal. Today. https://doi.org/10.1016/j.cattod.2018.10.026

Chermahini AN, Omran MK, Dabbagh HA, Mohammadnezhad G, Teimouri A (2015) Application of a functionalized mesoporous silica catalyst to the synthesis of tetrazoles, New J. Chem. https://doi.org/10.1039/C5NJ00211G

Ciriminna R, Carà PD, Lopez-Sanchez JA, Pagliaro M (2014) Catalysis via Sol–Gel Acid Silicas: An Important Chemical Technology for 2nd Generation Biorefineries, ChemCatChem. https://doi.org/10.1002/cctc.201402503

Debasish Das, Jyh-Fu Lee, Cheng S (2001) Sulfonic acid functionalized mesoporous MCM-41 silica as a convenient catalyst for Bisphenol-A synthesis, Chem. Commun. https://doi.org/10.1039/B107155F

Díaz I, Márquez-Alvarez C, Mohino F, Pérez-Pariente J, Sastre E (2001) A novel synthesis route of well ordered, sulfur-bearing MCM-41 catalysts involving mixtures of neutral and cationic surfactants, Micropor. Mesopor. Mat. https://doi.org/10.1016/S1387-1811(01)00195-0

Díaz I, Mohino F, Blasco T, Sastre E, Pérez-Pariente J (2005) Influence of the alkyl chain length of HSO_3-R-MCM-41 on the esterification of glycerol with fatty acids, Micropor. Mesopor. Mat. https://doi.org/10.1016/j.micromeso.2004.11.011

Díaz I, Mohino F, Pérez-Pariente J, Sastre E (2001) Synthesis, characterization and catalytic activity of MCM-41-type mesoporous silicas functionalized with sulfonic acid, Appl. Catal. A-Gen. https://doi.org/10.1016/S0926-860X(00)00808-5

Ding J, Cui M, Ma T, Shao R, Xu W, Wang P (2018) Catalytic amination of glycerol with dimethylamine over different type ofheteropolyacid/Zr-MCM-41 catalysts, Molecular Catalysis. https://doi.org/10.1016/j.mcat.2018.07.017

Ferreira ARO, Silvestre-Albero J, Maier ME, Ricardo NMPS, Cavalcante Jr CL, Luna FMT (2020) Sulfonated activated carbons as potential catalysts for biolubricant synthesis, Molecular Catalysis. https://doi.org/10.1016/j.mcat.2020.110888

González MD, Cesteros Y, Llorca J, Salagre P (2012) Boosted selectivity toward high glycerol tertiary butyl ethers by microwave-assisted sulfonic acid-functionalization of SBA-15 and beta zeolite, J. Catal. http://dx.doi.org/10.1016/j.jcat.2012.03.019

Huang Y, Chao PY, Cheng TY, Ho Y, Lin CT, Hsu HY, Wong JJ, Tsai TC (2016) Design of sulfonated mesoporous silica catalyst for fructose dehydration guided by difructose anhydride intermediate incorporated reaction network, Chem. Eng. J. https://doi.org/10.1016/j.cej.2015.08.031

Jagiello J, Thommes M (2004) Comparison of DFT characterization methods based on N_2, Ar, CO_2, and H_2 adsorption applied to carbons with various pore size distributions, Carbon. https://doi.org/10.1016/j.carbon.2004.01.022

Kister O, Roessner F (2012) Synthesis and characterization of mesoporous and amorphous silica modified with silica-organo-sulfogroups, J. Porous Mater.https://doi.org/10.1007/s10934-011-9455-z

Krishna NV, Anuradha S, Ganesh R, Kumar VV, Selvam P (2018) Sulfonic Acid Functionalized Ordered Mesoporous Silica and their Application as Highly Efficient and Selective Heterogeneous Catalysts in the Formation of 1,2 - Monoacetone - D - glucose, ChemCatChem. https://doi.org/10.1002/cctc.201801462

Liu Y, Chen J, Yao J, Yong Lu, Zhang L, Liu X (2009) Preparation and properties of sulfonated carbon–silica composites from sucrose dispersed on MCM-48, Chem. Eng. J. https://doi.org/10.1016/j.cej.2009.01.010

Madankar CS, Dalai AK, Naik SN (2013) Green synthesis of biolubricant base stock from canola oil. Industrial Crops and Products. http://dx.doi.org/10.1016/j.indcrop.2012.11.012

Mohino F, Diaz I, Pérez-Pariente J, Sastre E (2002) Synthesis, characterisation and catalytic activity of SO_3H-phenyl-MCM-41 materials, Stud. Surf. Sci. Catal. https://doi.org/10.1016/S0167-2991(02)80290-7

Noda Y, Li K, Engler AM, Elliott WA, Rioux RM (2016) Development of a robust sulfur quantification and speciation method for SBA-15-supported sulfonic acid catalysts, Catal. Sci. Technol. https://doi.org/10.1039/C6CY00292G

Oliveira JEL, Silveira MIGT, Costa MTA, Sousa JRM, Alves MCB, Junior SGJ (2020) Study of the Influence of 2-Ethylhexanol on the Determination of Acidity in Esterification Reactions with Caprylic Acid. Braz. J. of Develop. https://doi.org/10.34117/bjdv6n9-425

Owuna FJ, Dabai MU, Sokoto MA, Dangoggo SM, Bagudo BU, Birnin-Yauri UA, Hassan LG, Sada I, Abubakar AL, Jibrin MS (2020) Chemical modification of vegetable oils for the production of biolubricants using trimethylolpropane: A review. Egyptian Journal of Petroleum. https://doi.org/10.1016/j.ejpe.2019.11.004

403 Pindit K, Thanapimmetha A, Saisriyoot M, Srinopakun P (2021) Biolubricant basestocks
404 synthesis using 5-step reaction from jatropha oil, soybean oil, and palm fatty acid distillate.
405 Industrial Crops and Products. https://doi.org/10.1016/j.indcrop.2021.113484
406 Piscopo CG, Buhler S, Sartori G, Maggi R (2012) Supported sulfonic acids: reusable catalysts for
407 more sustainable oxidative coupling of xanthene-like compounds with nucleophiles, Catal.
408 Sci. Technol. https://doi.org/10.1039/C2CY20428B
409 Radhakrishnan R, Wu J, Jaenicke S, Chuah GK (2011) Effects of Acidity and Pore Size
410 Constraints on Supported Niobium Oxide Catalysts for the Selective Formation of Glycerol
411 Monolaurate, ChemCatChem. https://doi.org/10.1002/cctc.201000300
412 Reyes GB, Dasog M, Xing Na M, Titova LV, Veinot JGC, Hegmann FA (2015) Charge transfer
413 state emission dynamics in blue-emitting functionalized silicon nanocrystals, Phys. Chem.
414 Chem. Phys. http://dx.doi.org/10.1039/C5CP04819B
415 Rossetto E, Zanette T, Rocha RS, Nicola BP, Perghera SBC, Bernardo-Gusmão K (2018) Effect
416 of aluminum on the mesoporous materials support of heterogenized Nickel β-diimine in
417 oligomerization reactions, Molecular Catalysis. https://doi.org/10.1016/j.mcat.2018.05.026
418 Russo V, Taddeo F, Cogliano T, Vitiello R, Esposito R, Tesser R, Salmi T, Di Serio M (2021)
419 Investigation of the intrinsic reaction kinetics and the mass transfer phenomena of nonanoic
420 acid esterification with 2-ethylhexanol promoted by sulfuric acid or Amberlite IR120.
421 Chemical Engineering Journal. https://doi.org/10.1016/j.cej.2020.127236
422 Saboya RMA, Cecilia JA, García-Sancho C, Sales AV, Luna FMT, Rodríguez-Castellón E,
423 Cavalcante Jr CL (2017) Assessment of commercial resins in the biolubricants production
424 from free fatty acids of castor oil. Catalysis Today.
425 https://doi.org/10.1016/j.cattod.2016.02.020
426 Saboya RMA, Cecilia JA, García-Sancho C, Sales AV, Luna FMT, Rodríguez-Castellón E,
427 Cavalcante Jr CL (2017) Synthesis of biolubricants by the esterification of free fatty acids

from castor oil with branched alcohols using cationic exchange resins as catalysts. Industrial Crops & Products. https://doi.org/10.1016/j.indcrop.2017.04.018

Salimon J, Salih N, Yousif E (2012) Biolubricant basestocks from chemically modified ricinoleic acid. J. of King Saud University-Science. https://doi.org/10.1016/j.jksus.2010.08.008

Tayade KN, Mishra M, Munusamy K, Somani RS (2015) Synthesis of aluminium triflate-grafted MCM-41 as a water-tolerant acid catalyst for the ketalization of glycerol with acetone, Catal. Sci. Technol. https://doi.org/10.1039/C4CY01396D

Thommes M, Kaneko K, Neimark AV, Olivier JP, Rodriguez-Reinoso F, Rouquerol J, Sing KSW (2015) Physisorption of gases, with special reference to the evaluation of surface area and pore size distribution (IUPAC Technical Report), Pure Appl. Chem. https://doi.org/10.1515/pac-2014-1117

Valle-Vigón P, Sevilla M, Fuertes AB (2012) Sulfonated mesoporous silica–carbon composites and their use as solid acid catalysts, Appl. Surf. Sci. http://dx.doi.org/10.1016/j.apsusc.2012.08.059

Vartuli JC, Schmitt KD, Kresge CT, Roth WJ, Leonowicz ME, McCullen SB, Hellring SD, Beck JS, Schlenker JL, Olson DH, Sheppard EW (1994) Effect of Surfactant/Silica Molar Ratios on the Formation of Mesoporous Molecular Sieves: Inorganic Mimicry of Surfactant Liquid-Crystal Phases and Mechanistic Implications, Chem. Mater. https://doi.org/10.1021/cm00048a018

Wagh KV, Gajengi AL, Rath D, Parida KM, Bhanage BM (2018) Sulphated Al-MCM-41: A simple, efficient and recyclable catalyst forsynthesis of substituted aryl ketones/olefins via alcohols addition to alkynesand coupling with styrenes, Molecular Catalysis. https://doi.org/10.1016/j.mcat.2018.03.023

Wang K, Hua Q, Dabin L, Zhiwen Y (2019) NCN-Pincer palladium complexes immobilized on MCM-41 molecular sieve: Application inα-arylation reactions, Molecular Catalysis. https://doi.org/10.1016/j.mcat.2018.10.024

Wang R, Wang J, Zi H, Xia Y, Wang H, Liu X (2017) Catalytic transfer hydrogenation of ethyl levulinate to γ-valerolactone over zirconium (IV) Schiff base complexes on mesoporous silica with isopropanol as hydrogen source, Molecular Catalysis. https://doi.org/10.1016/j.mcat.2017.07.026

Wang Z, Jiang Y, Rachwalik R, Liu Z, Shi J, Hunger M, Huang J (2013) One‐Step Room‐Temperature Synthesis of [Al]MCM‐41 Materials for the Catalytic Conversion of Phenylglyoxal to Ethylmandelate, ChemCatChem. https://doi.org/10.1002/cctc.201300375

461 **TABLE CAPTIONS**

462

463 **Table 1.** Textural properties of the MCM-41 and MCM-41/SO_3H samples.

464

465 **Table 2.** Selectivity in oleate esters for the esterification of oleic acid with octanol and 2-

466 ethylhexanol at 90 °C after 6 h.

467

468 **Table 1**

Catalysts	S_{BET} (m^2/g)	Total pore volume (cm^3/g)	d_{100}	a_0 (nm)
MCM-41	855	0.71	1.50	1.73
MCM-41/SO_3H	600	0.39	1.49	1.72

469

470

471 **Table 2**

Esters / Catalysts	Selectivity (%)	
	Octyl oleate	**2-Ethylhexyl oleate**
MCM-41	76.0	63.8
MCM-41/SO_3H	87.0	89.3

472

473

SCHEME CAPTIONS

Scheme 1. Representation of sulfonic groups formation in MCM-41 by post-synthesis method.

Scheme 2. Esterification reaction of oleic acid with octanol (a) and 2-ethylhexanol (b).

Scheme 1

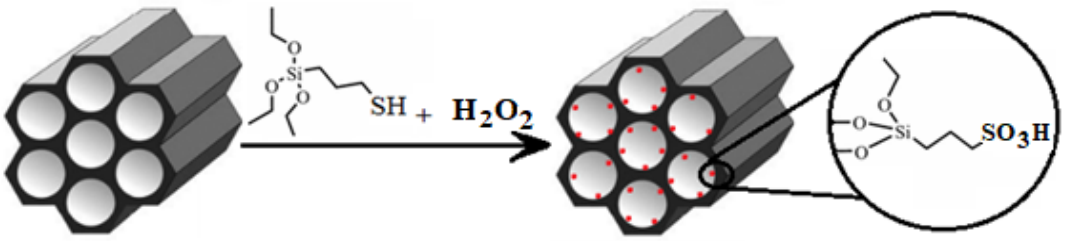

483 **Scheme 2**

484

(a)

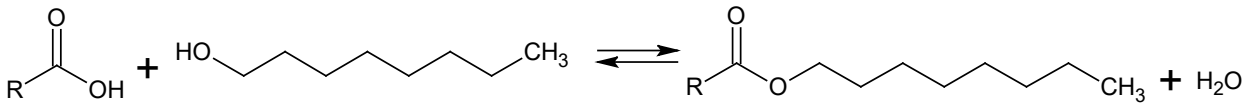

Octyl oleate

(b)

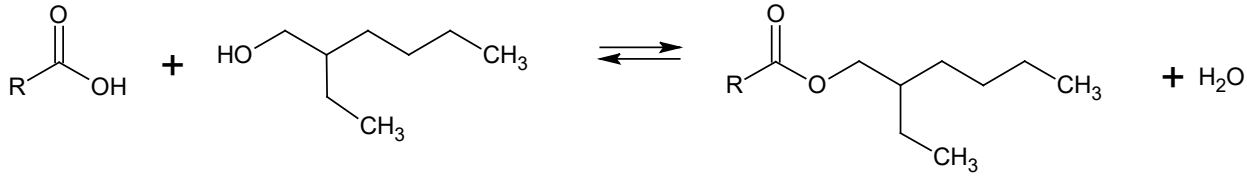

2-Ethylhexyl oleate

485 **FIGURE CAPTIONS**

486

487 **Figure 1.** (a) Nitrogen adsorption (full) and desorption (open) isotherm at -196 °C and (b) Pore
488 size distribution of the MCM-41 and MCM-41/SO_3H samples.

489

490 **Figure 2.** SEM images (a,b) and TEM images (c,d,e,f) of the MCM-41 and MCM-41/SO_3H.

491

492 **Figure 3.** XRD of the MCM-41 and MCM-41/SO_3H samples.

493

494 **Figure 4.** XPS spectrum of high-resolution S 2p of the MCM-41/SO_3H sample.

495

496 **Figure 5.** FTIR spectra of the MCM-41 and MCM 41/SO_3H sample.

497

498 **Figure 6.** TGA curves (black lines) and DTG curves (blue lines) in N_2 atmosphere: (a) MCM-
499 41 and (b) MCM-41/SO_3H.

500

501 **Figure 7.** ^1H NMR of product obtained from the esterification reaction with (a) octanol and (b)
502 2-ethylhexanol.

503

504 **Figure 8.** Oleic acid conversion values over time using (a) octanol and (b) 2-ethylhexanol.

505

Figure 1

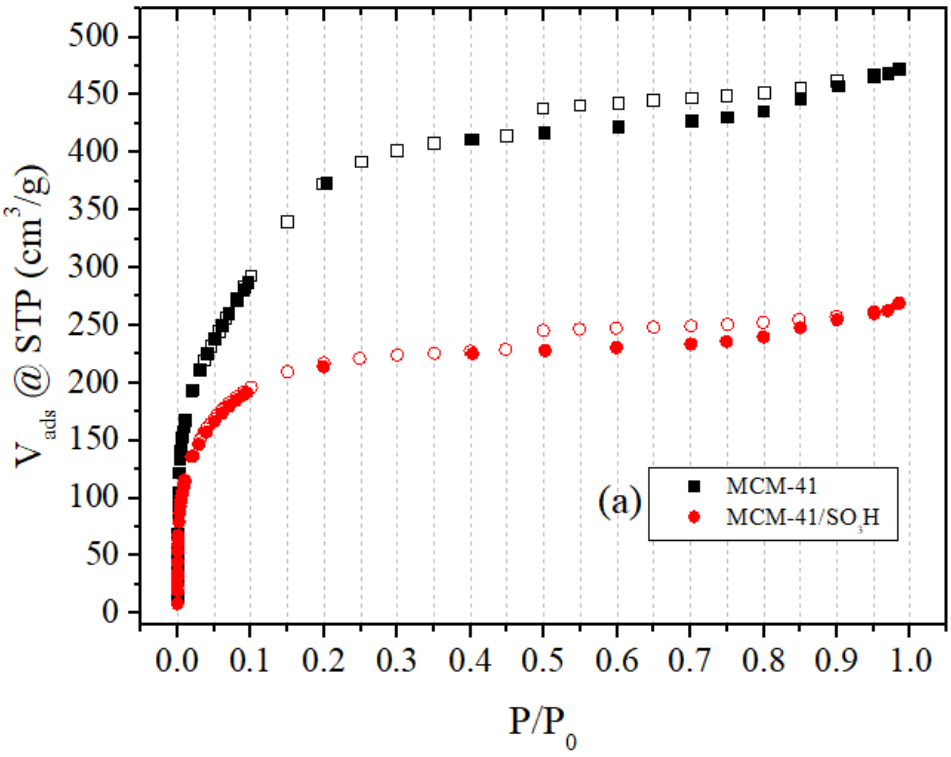

506

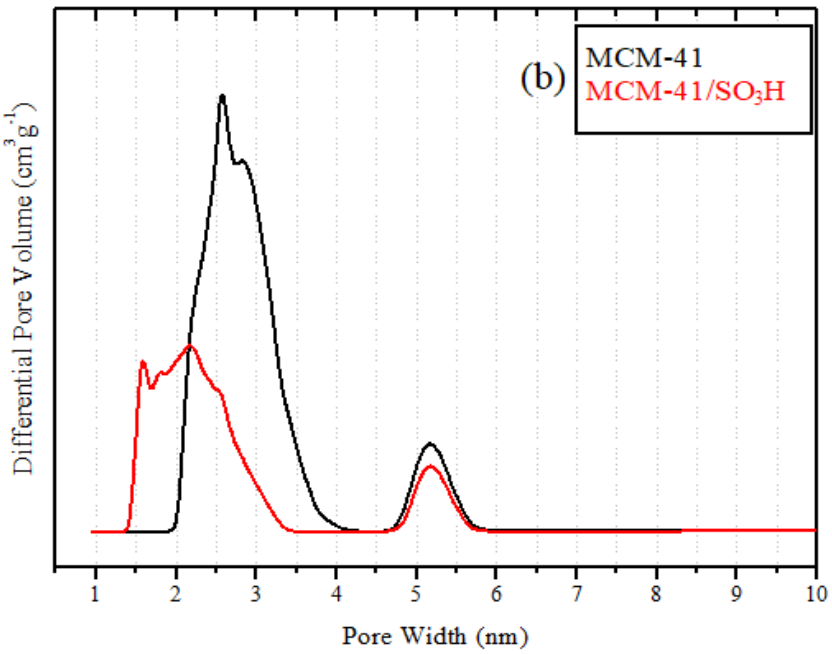

507

508

509

Figure 2

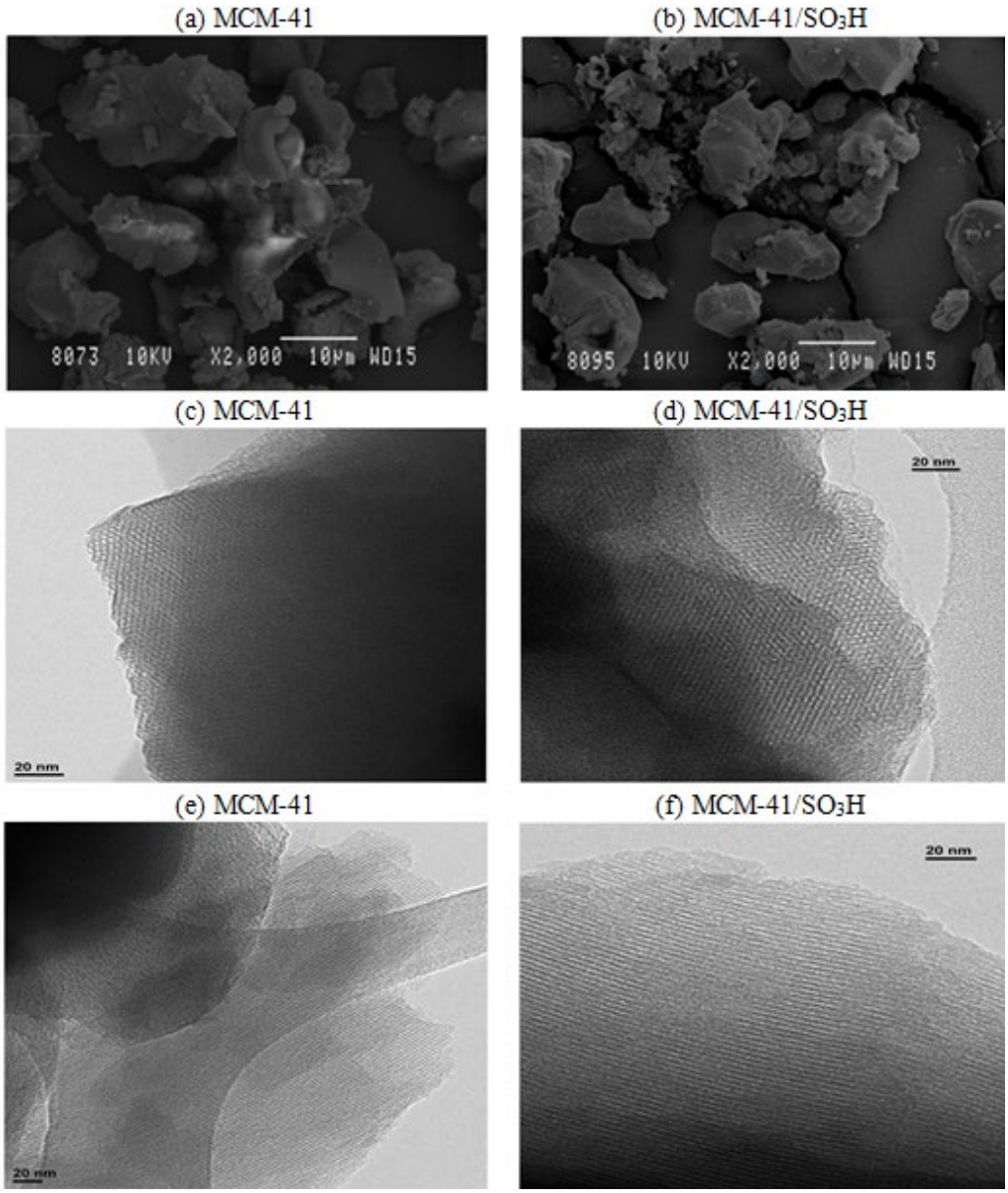

510

511

512 **Figure 3**

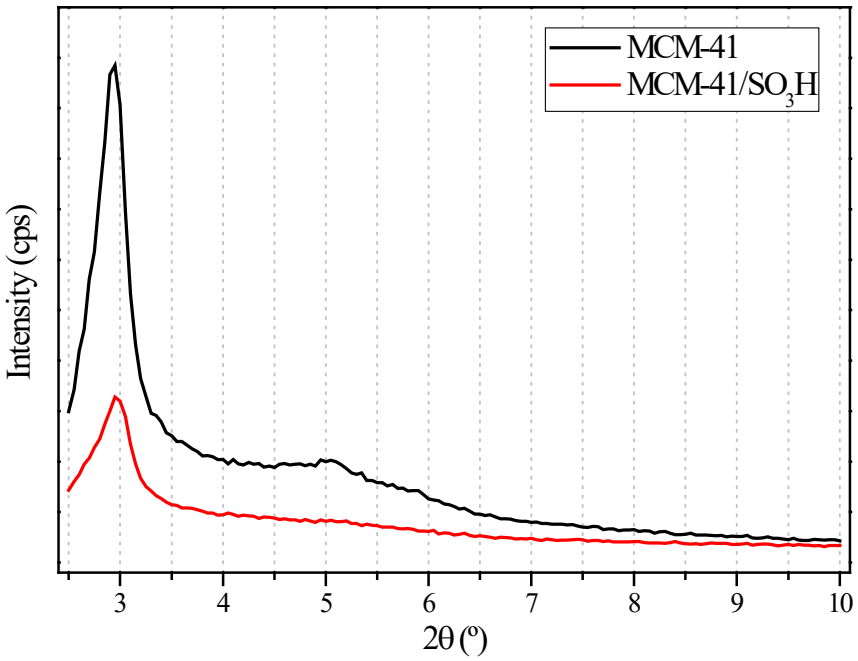

513

514

515

Figure 4

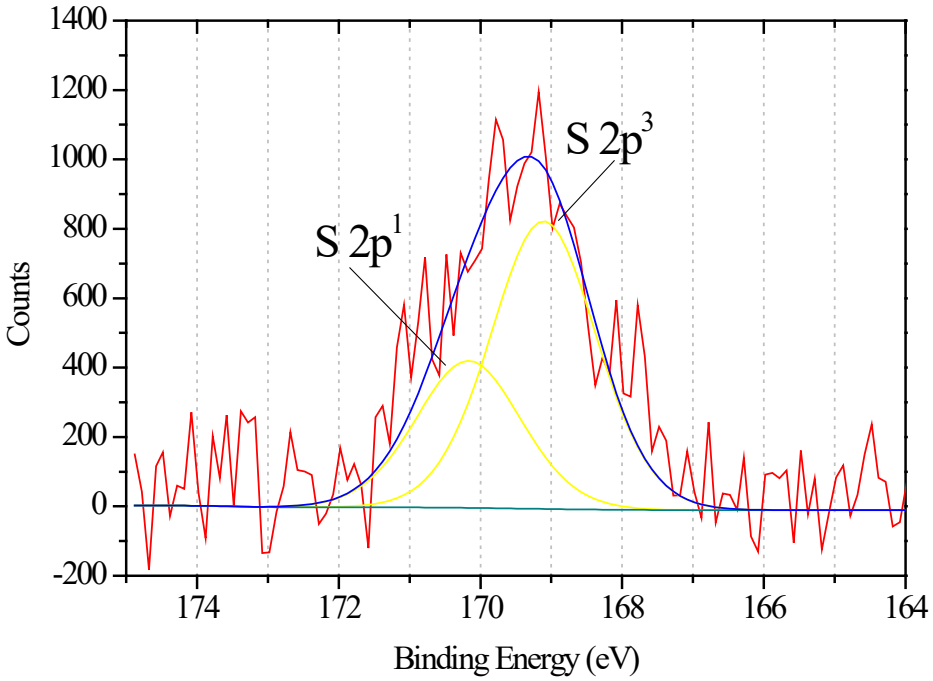

516

517

518

Figure 5

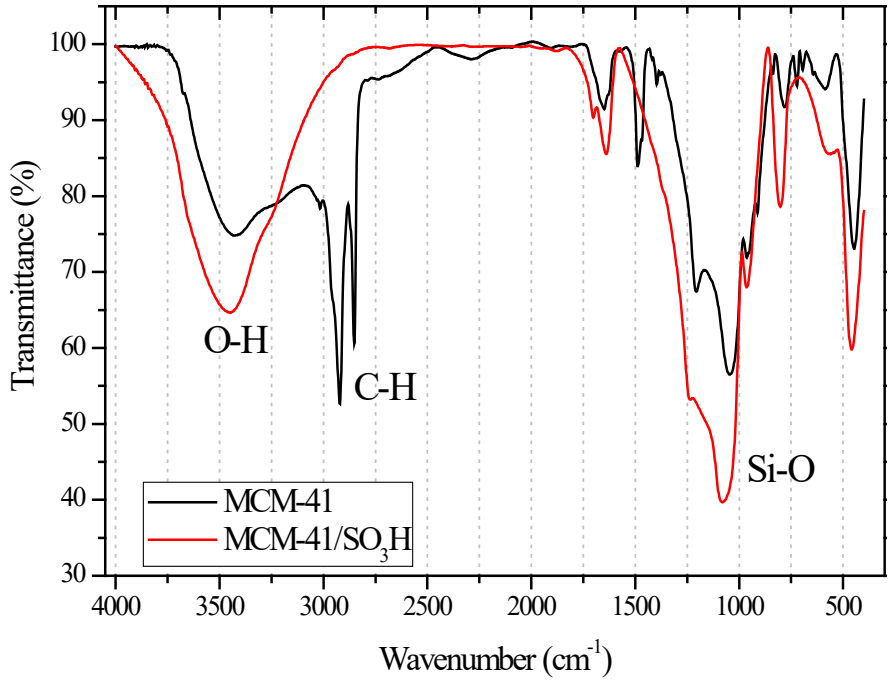

519

520

Figure 6

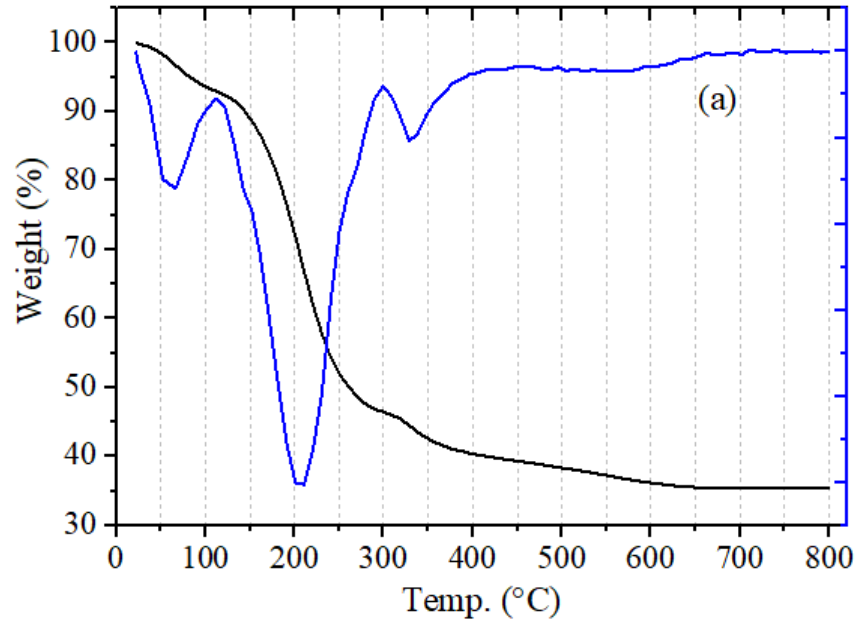
(a)
Weight (%)
Temp. (°C)
100
90
80
70
60
50
40
30
0
100
200
300
400
500
600
700
800

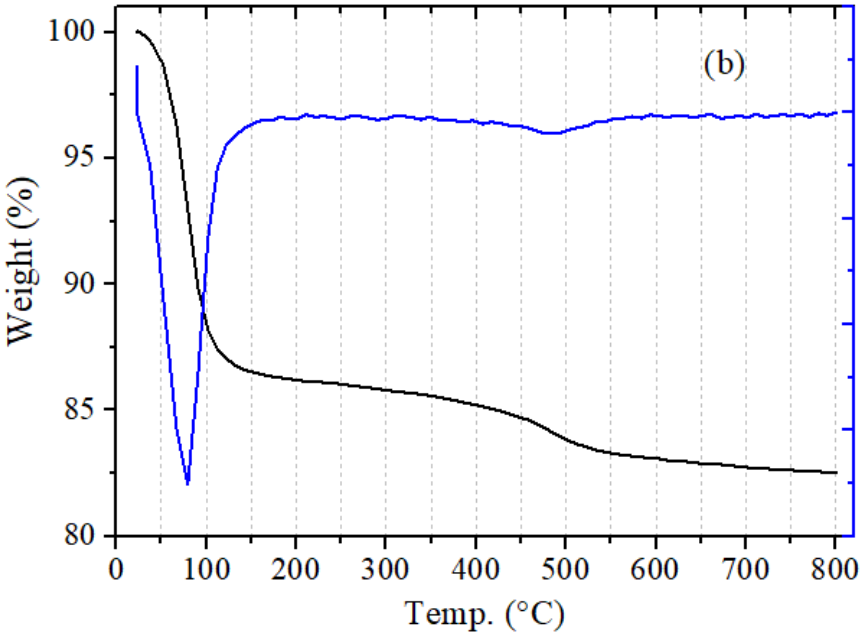
(b)
Weight (%)
Temp. (°C)
100
95
90
85
80
0
100
200
300
400
500
600
700
800

525

Figure 7

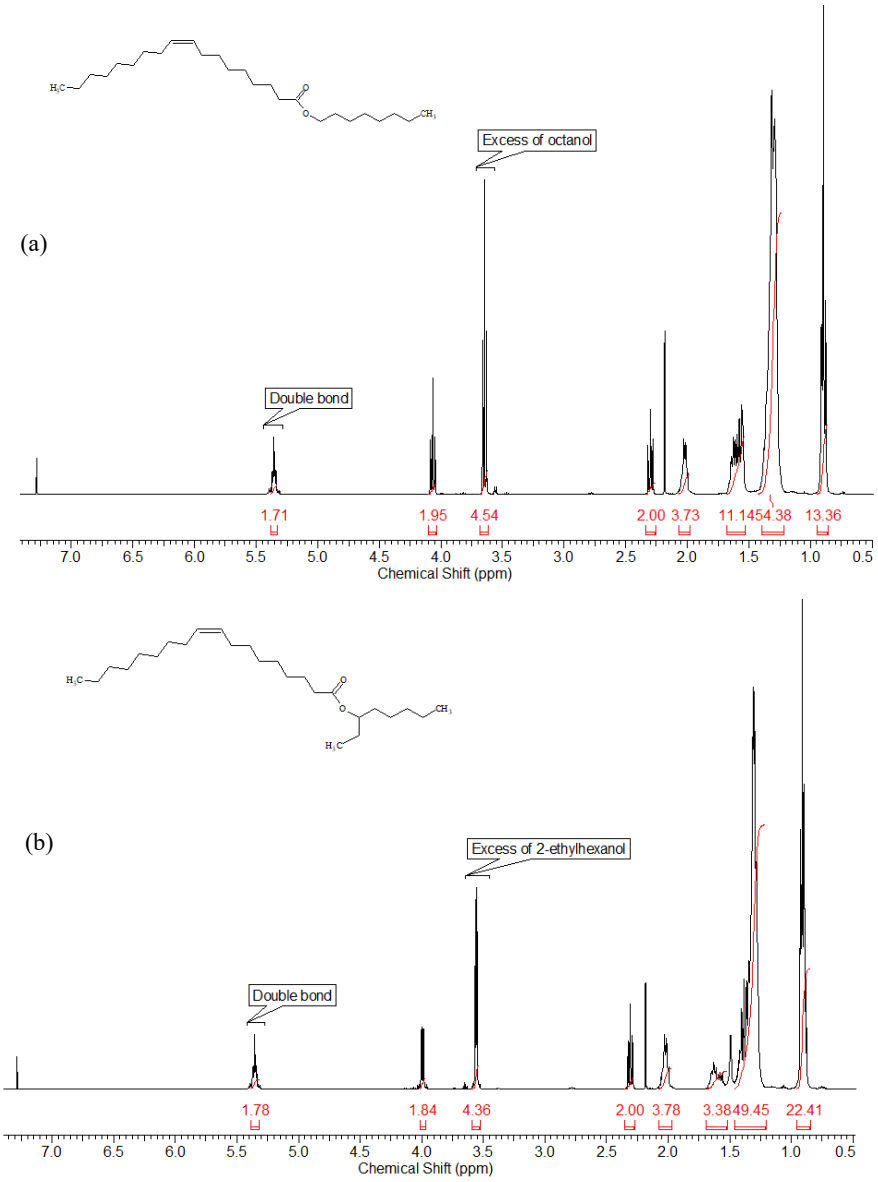

526

527

Figure 8

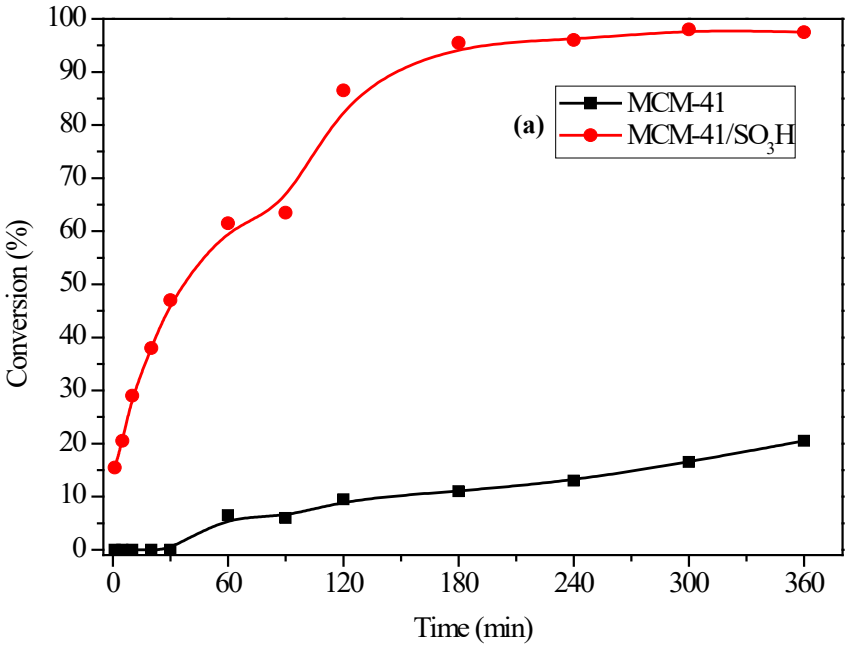

528

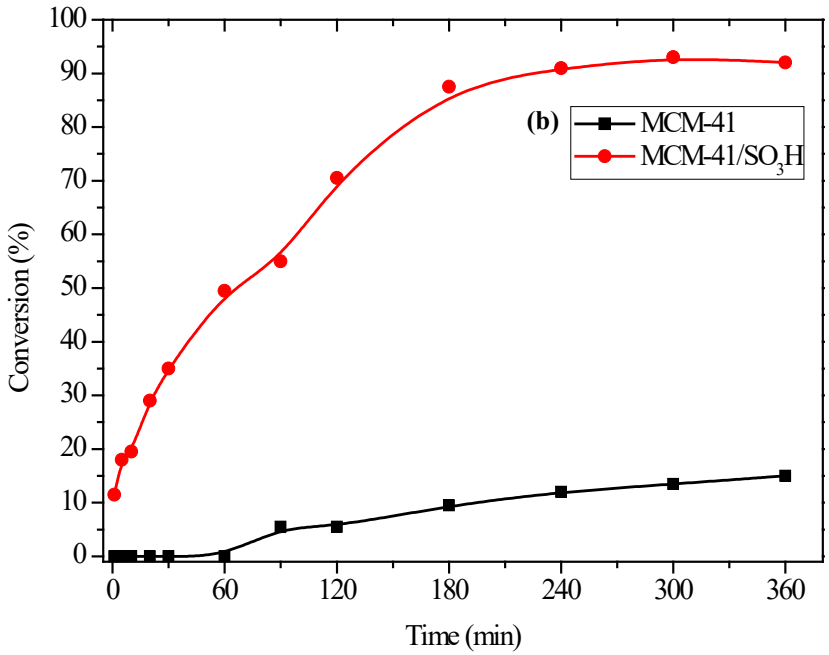

529